Acta Mech 230:1257–1273 (2019)
https://doi.org/10.1007/s00707-017-2028-8

ORIGINAL PAPER

Yang Li · Lian-zhi Yang · Yang Gao

An exact solution for a functionally graded multilayered one-dimensional orthorhombic quasicrystal plate

Received: 9 June 2017 / Published online: 23 December 2017

Abstract This paper investigates the problem of a functionally graded multilayered one-dimensional orthorhombic quasicrystal plate with simply supported edge conditions. Assuming that the functionally graded material properties vary exponentially along the thickness direction, a solution for a functionally graded plate subjected to top surface loading is obtained by using the pseudo-Stroh formalism. The propagator matrix method is utilized to get the solution for the corresponding multilayered case. The exact solution is applied to a multilayered plate made of quasicrystals and crystals. The influences of the exponential factor, load form, and stacking sequence on physical quantities are studied in numerical examples. The exact solution can be used to design a functionally graded multilayered plate composed of one-dimensional quasicrystals and crystals. The numerical results can also serve as a basis for other numerical methods, such as finite element and boundary element methods.

1 Introduction

With the first discovery of icosahedral quasicrystals (QCs) in Al–Mn alloys by Shechtman in the early 1980s, QCs caused a revolutionary breakthrough in the field of crystallography [1–3]. QCs have a new symmetry, which is quasiperiodic symmetry, and their structures have a long-range quasiperiodic translational order and a long-range orientational order [4]. One-dimensional (1D) QCs refer to a three-dimensional solid with atomic arrangement which is periodic in a plane and quasiperiodic in the direction normal to this plane. Because of the nonperiodic structure, QCs have many special properties, such as low friction coefficient, low adhesion, high wear resistance, low level of porosity and so on. By taking advantage of the properties of QCs, they can be used as coatings or films of metals, and as strengthening phases to reinforce alloys in industry [5,6].

Multilayered structures, which are usually bonded together by two or more plates and beams, have been extensively applied to engineering practices. The analyses for static and dynamic characteristics have been proposed [7,8]. Multilayered plates [9–11] and beams [12,13] are the main research objects in the study of

Y. Gao (✉)
College of Science, China Agricultural University, Beijing 100083, China
E-mail: gaoyangg@gmail.com

Y. Li
College of Engineering, China Agricultural University, Beijing 100083, China

L. Yang
School of Civil and Resource Engineering, University of Science and Technology Beijing, Beijing 100083, China

Y. Li
Department of Mechanical and Power Engineering, Yingkou Institute of Technology, Yingkou 115014, China

layered structures. The bonding of different materials will cause some drawbacks in joints, such as stress concentration and micro-crack. These defects will limit the application of multilayered structures.

In order to overcome these defects, functionally gradient material (FGM) can be used. FGM has continuously varying material properties along one direction. Due to the vital importance of FGM, it has attracted the general scientists' interest. Axisymmetric bending of FGPM circular plates based on three-dimensional theory of piezoelectricity has been investigated [14]. Peng and Li [15] studied the thermo-elastic analysis of a functionally graded annulus with arbitrary gradient. Pan and Han [16] derived the exact solution for functionally graded layered magneto-electro-elastic plates. Yan and Jiang [17] solved the parallel dielectric crack problem in functionally graded piezoelectric materials. The exact solutions for multidirectional functionally graded plates were sought for the thickness domain using the state-space method [18]. Based on the transfer matrix method, Bian et al. [19] determined the shape function and then obtained the analytical solutions for single span and multispan functionally graded plates in cylindrical bending. The modified couple stress theory was employed to analyze the size-dependent behavior of the three-dimensional FGM anisotropic elastic composites under the surface load [20]. Zhong et al. [21] summarized the recent advances in the study on functionally graded materials and structures, and the future development of mechanic analysis of them was given. However, to the authors' knowledge, little study regarding a functionally graded multilayered QC plate has been done until now.

The pseudo-Stroh formalism [7] is used to get the solution for an FGM 1D QC plate, and the propagator matrix method is then utilized to solve the multilayered case. Two different load forms, a normal load and a shear load, are studied. The effects of the exponential factor and stacking sequence on physical quantities are compared in both examples. The numerical results can reveal the static behavior of a functionally graded multilayered 1D QC plate and serve as a basis for other numerical methods, such as finite element and boundary element methods.

2 Basic equations

A rectangular Cartesian coordinate system (x_1, x_2, x_3) is used to describe a 1D QC plate whose atomic arrangement is quasiperiodic along the x_3 direction and periodic in the x_1-x_2 plane. In this paper, 1D orthorhombic QCs with the point groups 2_h2_h2, $mm2$, 2_hmm_h, mmm_h are studied. We can get the strain–displacement relations for 1D QCs from the linear elastic theory of QCs [22],

$$\varepsilon_{ij} = \left(\partial_j u_i + \partial_i u_j\right)/2,\ w_{3j} = \partial_j w_3, \tag{1}$$

where $i,\ j = 1, 2, 3$ and repeated indices imply the summation from 1 to 3, ε_{ij} and w_{3j} denote the phonon and phason strains, respectively, and u_i and w_3 represent the phonon and phason displacements, respectively; $\partial_j = \partial/\partial x_j$.

In the absence of body forces, the static equilibrium equations can be expressed as

$$\partial_j \sigma_{ij} = 0,\ \partial_j H_{3j} = 0, \tag{2}$$

where σ_{ij} and H_{3j} denote the stress components in the phonon and phason fields, respectively.

The linear constitutive equations for 1D orthorhombic QCs can be expressed as [23]:

$$\begin{aligned}
\sigma_{11} &= C_{11}\varepsilon_{11} + C_{12}\varepsilon_{22} + C_{13}\varepsilon_{33} + R_1 w_{33},\\
\sigma_{22} &= C_{12}\varepsilon_{11} + C_{22}\varepsilon_{22} + C_{23}\varepsilon_{33} + R_2 w_{33},\\
\sigma_{33} &= C_{13}\varepsilon_{11} + C_{23}\varepsilon_{22} + C_{33}\varepsilon_{33} + R_3 w_{33},\\
\sigma_{23} &= \sigma_{32} = 2C_{44}\varepsilon_{23} + R_5 w_{32},\\
\sigma_{31} &= \sigma_{13} = 2C_{55}\varepsilon_{31} + R_6 w_{31},\\
\sigma_{12} &= \sigma_{21} = 2C_{66}\varepsilon_{12},\\
H_{33} &= R_1\varepsilon_{11} + R_2\varepsilon_{22} + R_3\varepsilon_{33} + K_3 w_{33},\\
H_{32} &= 2R_5\varepsilon_{23} + K_2 w_{32},\\
H_{31} &= 2R_6\varepsilon_{31} + K_1 w_{31},
\end{aligned} \tag{3}$$

where C_{ij}, C_{44}, C_{55}, C_{66} denote the elastic constants in the phonon field, K_i represent the elastic constants in the phason field, and $R_m (m = 1, 2, 3, 5, 6)$ indicate the phonon–phason coupling elastic constants.

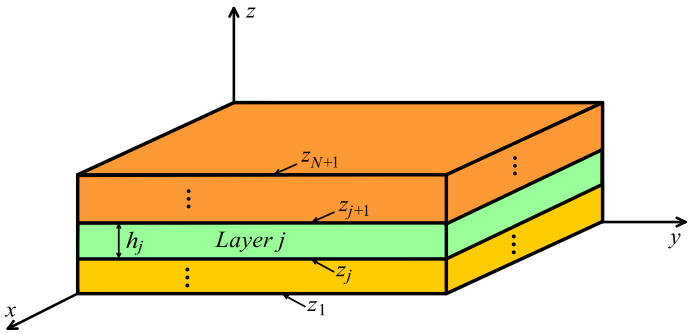

Fig. 1 A functionally graded multilayered 1D QC plate

The material properties of FGM are exponentially distributed along the x_3-direction. Therefore, the material coefficients in Eq. (3) can be expressed in the following form:

$$C_{ij}(x_3) = C_{ij}^0 \mathrm{e}^{\eta x_3}, \quad R_m(x_3) = R_m^0 \mathrm{e}^{\eta x_3}, \quad K_i(x_3) = K_i^0 \mathrm{e}^{\eta x_3}, \tag{4}$$

where η is the exponential factor characterizing the degree of the material gradient in the x_3-direction, and the superscript 0 is attached to indicate the x_3-independent factors in the material coefficients. When $\eta = 0$, the material coefficients for the FGM correspond to a homogeneous material [24].

3 Problem description and general solution

As shown in Fig. 1, a functionally graded multilayered 1D orthorhombic QC plate with horizontal dimensions $x \times y = L_x \times L_y$ and a total thickness $z = H$ is studied, which is in a rectangular Cartesian coordinate system (x, y, z) with its four sides being simply supported. Let j denote the j-th layer of the layered plate. For layer j, its lower and upper interfaces are at z_j and z_{j+1}, respectively. Hence, it is apparent that $z_1 = 0$ and $z_{N+1} = H$. The displacements and z-direction traction stresses along the interfaces are assumed to be continuous.

For a FGM 1D QC plate, the solution of the extended displacement vector takes the following form:

$$\mathbf{u} = \begin{Bmatrix} u_x \\ u_y \\ u_z \\ w_z \end{Bmatrix} = \mathrm{e}^{sz} \begin{Bmatrix} a_1 \cos px \sin qy \\ a_2 \sin px \cos qy \\ a_3 \sin px \sin qy \\ a_4 \sin px \sin qy \end{Bmatrix}, \tag{5}$$

where

$$p = n\pi/L_x, \quad q = m\pi/L_y, \tag{6}$$

with n and m being two positive integers. s is the eigenvalue, a_1, a_2, a_3, a_4 are the components of the corresponding eigenvector, and the eigenvalue and the corresponding eigenvector are to be determined. Only one term of a double Fourier series expansion with summations for n and m is considered in Eq. (5).

The simply supported displacement boundary conditions of a functionally graded multilayered QC plate are given by

$$\begin{aligned} u_y = u_z = w_z = 0 \quad &\text{at } x = 0 \quad \text{and } x = L_x, \\ u_x = u_z = w_z = 0 \quad &\text{at } y = 0 \quad \text{and } y = L_y. \end{aligned} \tag{7}$$

Inserting Eq. (5) into the constitutive equation (3) yields the extended traction vector as

$$\mathbf{t} = \begin{Bmatrix} \sigma_{xz} \\ \sigma_{yz} \\ \sigma_{zz} \\ H_{zz} \end{Bmatrix} = \mathrm{e}^{(s+\eta)z} \begin{Bmatrix} b_1 \cos px \sin qy \\ b_2 \sin px \cos qy \\ b_3 \sin px \sin qy \\ b_4 \sin px \sin qy \end{Bmatrix}. \tag{8}$$

Two vectors which are the coefficients in Eqs. (5) and (8) can be written as

$$\mathbf{a} = \{a_1, a_2, a_3, a_4\}^{\mathrm{T}}, \quad \mathbf{b} = \{b_1, b_2, b_3, b_4\}^{\mathrm{T}}, \tag{9}$$

where the superscript T denotes the transpose of a vector or matrix.

Using Eq. (3), the relation between the vectors **a** and **b** can be easily derived as follows:

$$\mathbf{b} = \left(-\mathbf{P}^{\mathrm{T}} + s\mathbf{T}\right)\mathbf{a}, \tag{10}$$

where

$$\mathbf{P} = \begin{bmatrix} 0 & 0 & C_{13}^0 p & R_1^0 p \\ 0 & 0 & C_{23}^0 q & R_2^0 q \\ -C_{55}^0 p & -C_{44}^0 q & 0 & 0 \\ -R_6^0 p & -R_5^0 q & 0 & 0 \end{bmatrix}, \quad \mathbf{T} = \begin{bmatrix} C_{55}^0 & 0 & 0 & 0 \\ 0 & C_{44}^0 & 0 & 0 \\ 0 & 0 & C_{33}^0 & R_3^0 \\ 0 & 0 & R_3^0 & K_3^0 \end{bmatrix}. \tag{11}$$

The other stress components in Eq. (3) can be expressed as

$$\begin{Bmatrix} \sigma_{xx} \\ \sigma_{xy} \\ \sigma_{yy} \\ H_{zx} \\ H_{zy} \end{Bmatrix} = \mathrm{e}^{(s+\eta)z} \begin{Bmatrix} c_1 \sin px \sin qy \\ c_2 \cos px \cos qy \\ c_3 \sin px \sin qy \\ c_4 \cos px \sin qy \\ c_5 \sin px \cos qy \end{Bmatrix}, \tag{12}$$

where

$$\begin{Bmatrix} c_1 \\ c_2 \\ c_3 \\ c_4 \\ c_5 \end{Bmatrix} = \begin{bmatrix} -C_{11}^0 p & -C_{12}^0 q & C_{13}^0 s & -R_1^0 s \\ C_{66}^0 q & C_{66}^0 p & 0 & 0 \\ -C_{12}^0 p & -C_{22}^0 q & C_{23}^0 s & R_2^0 s \\ R_6^0 s & 0 & R_6^0 p & K_1^0 p \\ 0 & R_5^0 s & R_5^0 q & K_2^0 q \end{bmatrix} \begin{Bmatrix} a_1 \\ a_2 \\ a_3 \\ a_4 \end{Bmatrix}. \tag{13}$$

Substituting Eqs. (8) and (12) into the equilibrium equation (2), we get the following eigenequation:

$$\left[\mathbf{Q} - \eta\mathbf{P}^{\mathrm{T}} + s\left(\mathbf{P} - \mathbf{P}^{\mathrm{T}} + \eta\mathbf{T}\right) + s^2\mathbf{T}\right]\mathbf{a} = \mathbf{0}, \tag{14}$$

where **Q** takes the following form:

$$\mathbf{Q} = \begin{bmatrix} -\left(C_{11}^0 p^2 + C_{66}^0 q^2\right) & -pq\left(C_{12}^0 + C_{66}^0\right) & 0 & 0 \\ -pq\left(C_{12}^0 + C_{66}^0\right) & -\left(C_{22}^0 q^2 + C_{66}^0 p^2\right) & 0 & 0 \\ 0 & 0 & -\left(C_{55}^0 p^2 + C_{44}^0 q^2\right) & -\left(R_6^0 p^2 + R_5^0 q^2\right) \\ 0 & 0 & -\left(R_6^0 p^2 + R_5^0 q^2\right) & -\left(K_1^0 p^2 + K_2^0 q^2\right) \end{bmatrix}. \tag{15}$$

It is remarkable that Eq. (14), if the exponential factor $\eta = 0$, degenerates into the eigenequation for the corresponding homogeneous case [7].

In view of Eqs. (10) and (14), we can take the vector **b** as

$$\mathbf{b} = -\frac{1}{s+\eta}\left(\mathbf{Q} + s\mathbf{P}\right)\mathbf{a}. \tag{16}$$

Then, utilizing Eqs. (10) and (16), Eq. (14) can be rewritten into a 8×8 linear eigensystem

$$\mathbf{N}\xi = s\xi, \xi = \{\mathbf{a}, \mathbf{b}\}^{\mathrm{T}}, \tag{17}$$

where

$$\mathbf{N} = \begin{bmatrix} \mathbf{T}^{-1}\mathbf{P}^{\mathrm{T}} & \mathbf{T}^{-1} \\ -\mathbf{Q} - \mathbf{P}\mathbf{T}^{-1}\mathbf{P}^{\mathrm{T}} & -\mathbf{P}\mathbf{T}^{-1} - \eta\mathbf{I} \end{bmatrix}, \tag{18}$$

and **I** in Eq. (18) is the 4×4 unit matrix. The eigenvalues s can be obtained through making the determinant of the characteristic matrix in Eq. (17) zero. The corresponding eigenvectors ξ are determined from Eq. (17). If repeated roots occur, a slight change in the material constants would cause distinct roots with negligible error [25]. Consequently, we only consider the case of different eigenvalues.

It is assumed that the first four eigenvalues have positive real parts (if the root is purely imaginary, we will pick up the one with positive imaginary part) and the remainder have the relation with the first four as

$$s_{\alpha+4} = -s_\alpha - \eta, \quad \mathrm{Re}\,(s_\alpha) > 0 \quad (\alpha = 1, 2, 3, 4), \tag{19}$$

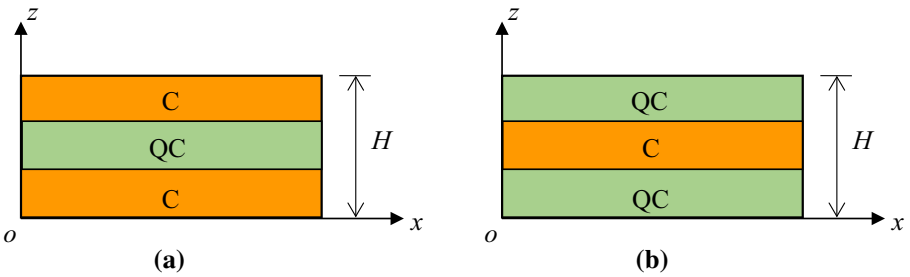

Fig. 2 Stacking sequence **a** C/QC/C. **b** QC/C/QC

Table 1 Material coefficients of the Al–Ni–Co (C_{ij}^0 in 10^9 N/m^2, R_m^0 in 10^9 N/m^2, K_i^0 in 10^9 N/m^2)

$C_{11}^0 = C_{22}^0$	C_{12}^0	$C_{13}^0 = C_{23}^0$	C_{33}^0	$C_{44}^0 = C_{55}^0$	$C_{66}^0 = (C_{11}^0 - C_{22}^0)/2$
234.3	57.4	66.6	23.2	70.2	88.5
$R_1^0 = R_2^0 = R_3^0 = R_5^0 = R_6^0$			$K_1^0 = K_2^0$		K_3^0
8.85			12.2		2.4

Table 2 Material coefficients of the $BaTiO_3$ (C_{ij}^0 in 10^9 N/m^2, R_m^0 in 10^9 N/m^2, K_i^0 in 10^9 N/m^2)

$C_{11}^0 = C_{22}^0$	C_{12}^0	$C_{13}^0 = C_{23}^0$	C_{33}^0	$C_{44}^0 = C_{55}^0$	$C_{66}^0 = (C_{11}^0 - C_{22}^0)/2$
166	77	7. 8	162	43	44.5
$R_1^0 = R_2^0 = R_3^0 = R_5^0 = R_6^0$			$K_1^0 = K_2^0 = K_3^0$		
0			0		

in which Re indicates the real part of a quantity. The general solution for the extended displacement vector **u** and traction vector (of the z-dependent factor) **t** are

$$\begin{pmatrix} \mathbf{u} \\ \mathbf{t} \end{pmatrix} = \begin{bmatrix} \mathbf{A}_1 \left\langle \mathrm{e}^{s^* z} \right\rangle & \mathbf{A}_2 \left\langle \mathrm{e}^{(-s^*-\eta)z} \right\rangle \\ \mathbf{B}_1 \left\langle \mathrm{e}^{(s^*+\eta)z} \right\rangle & \mathbf{B}_2 \left\langle \mathrm{e}^{-s^* z} \right\rangle \end{bmatrix} \begin{pmatrix} \mathbf{K}_1 \\ \mathbf{K}_2 \end{pmatrix}, \tag{20}$$

where

$$\begin{aligned} &\mathbf{A}_1 = [\mathbf{a}_1, \mathbf{a}_2, \mathbf{a}_3, \mathbf{a}_4], \mathbf{A}_2 = [\mathbf{a}_5, \mathbf{a}_6, \mathbf{a}_7, \mathbf{a}_8], \\ &\mathbf{B}_1 = [\mathbf{b}_1, \mathbf{b}_2, \mathbf{b}_3, \mathbf{b}_4], \mathbf{B}_2 = [\mathbf{b}_5, \mathbf{b}_6, \mathbf{b}_7, \mathbf{b}_8], \\ &\left\langle \mathrm{e}^{s^* z} \right\rangle = \mathrm{diag}\left[\mathrm{e}^{s_1 z}, \mathrm{e}^{s_2 z}, \mathrm{e}^{s_3 z}, \mathrm{e}^{s_4 z}\right], \end{aligned} \tag{21}$$

$\mathbf{K}_1$ and $\mathbf{K}_2$ are two 4×1 constant column matrices to be determined according to the boundary conditions.

Equation (20) is the general solution for a simply supported FGM 1D QC plate. If $\eta = 0$, Eq. (20) is same with the general solution for the corresponding homogeneous case [24]. Then, the propagator matrix is introduced to get the solution for a multilayered case. The propagator matrix method is useful for the layered structures and has certain advantages in the calculation [26,27].

Using Eq. (20), the column coefficient matrices $\mathbf{K}_1$ and $\mathbf{K}_2$ can be obtained as

$$\begin{pmatrix} \mathbf{K}_1 \\ \mathbf{K}_2 \end{pmatrix}_j = \begin{bmatrix} \mathbf{A}_1 \left\langle \mathrm{e}^{s^*(z-z_j)} \right\rangle & \mathbf{A}_2 \left\langle \mathrm{e}^{(-s^*-\eta)(z-z_j)} \right\rangle \\ \mathbf{B}_1 \left\langle \mathrm{e}^{(s^*+\eta)(z-z_j)} \right\rangle & \mathbf{B}_2 \left\langle \mathrm{e}^{-s^*(z-z_j)} \right\rangle \end{bmatrix}_j^{-1} \begin{pmatrix} \mathbf{u} \\ \mathbf{t} \end{pmatrix}_j, \tag{22}$$

where the subscript j denotes layer $j$and s^* indicates the eigenvalues of layer j, and $z_j \le z \le z_{j+1}$. Let z be equal to z_j and z_{j+1}, respectively, then the column matrices can be rewritten as

$$\begin{pmatrix} \mathbf{K}_1 \\ \mathbf{K}_2 \end{pmatrix}_j = \begin{bmatrix} \mathbf{A}_1 & \mathbf{A}_2 \\ \mathbf{B}_1 & \mathbf{B}_2 \end{bmatrix}_j^{-1} \begin{pmatrix} \mathbf{u} \\ \mathbf{t} \end{pmatrix}_{z_j} = \begin{bmatrix} \mathbf{A}_1 \left\langle \mathrm{e}^{s^* h_j} \right\rangle & \mathbf{A}_2 \left\langle \mathrm{e}^{(-s^*-\eta)h_j} \right\rangle \\ \mathbf{B}_1 \left\langle \mathrm{e}^{(s^*+\eta)h_j} \right\rangle & \mathbf{B}_2 \left\langle \mathrm{e}^{-s^* h_j} \right\rangle \end{bmatrix}_j^{-1} \begin{pmatrix} \mathbf{u} \\ \mathbf{t} \end{pmatrix}_{z_{j+1}}, \tag{23}$$

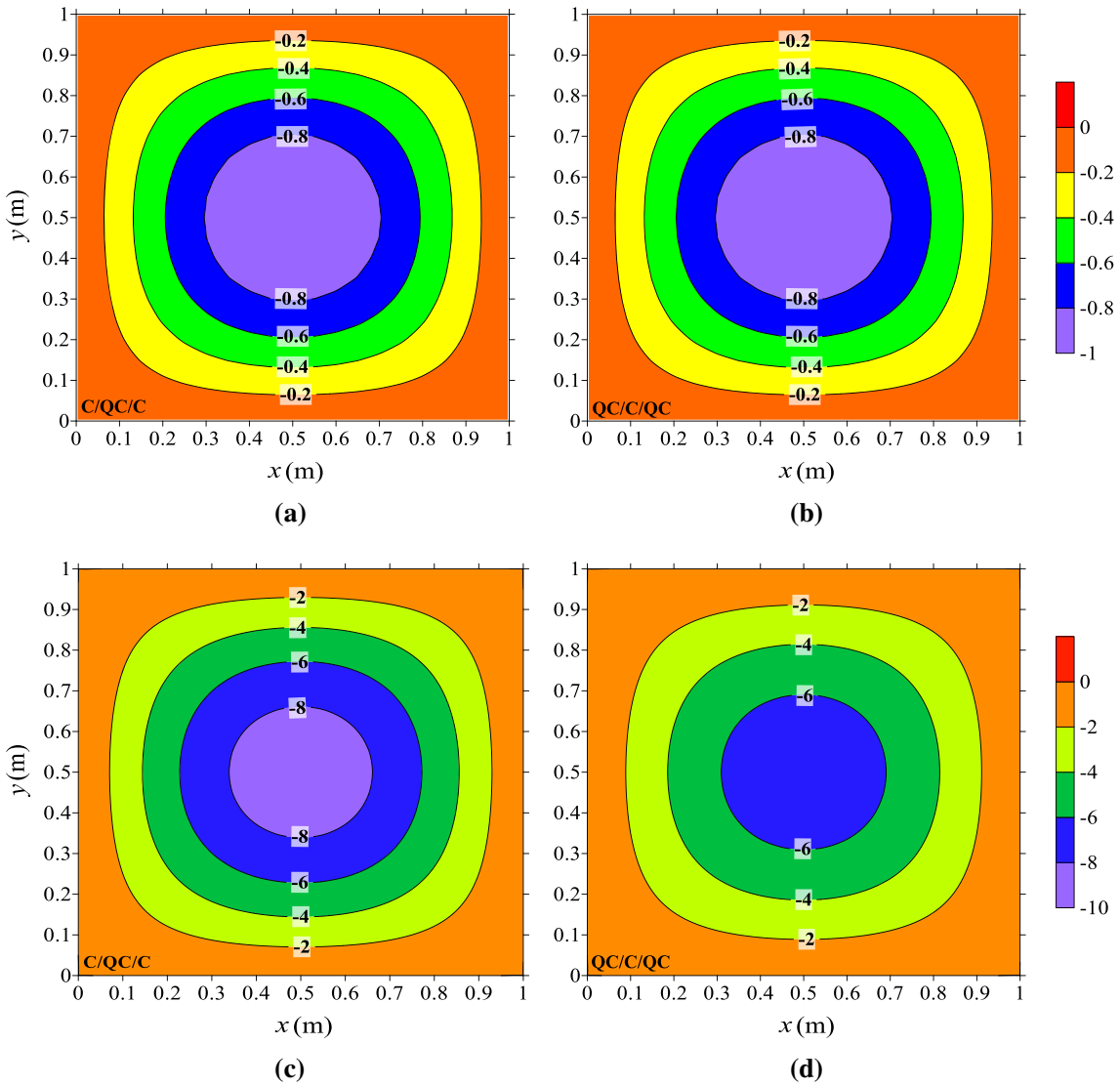

Fig. 3 Contour plots of physical quantities at the top surfaces ($z = 0.3$ m) subjected to a normal load with $\eta = 5$. **a** σ_{zz} for the C/QC/C plate (N/m^2), **b** σ_{zz} for the QC/C/QC plate (N/m^2), **c** u_z for the C/QC/C plate (10^{-12} m), **d** u_z for the QC/C/QC plate (10^{-12} m)

in which $h_j = z_{j+1} - z_j$ is the thickness of layer j.

Furthermore, in terms of the lower surface of layer j, the displacement vector $\mathbf{u}$ and traction vector $\mathbf{t}$ on the upper surface can be expressed as

$$\begin{pmatrix} \mathbf{u} \\ \mathbf{t} \end{pmatrix}_{z_{j+1}} = \begin{bmatrix} \mathbf{A}_1 \left\langle \mathrm{e}^{s^* h_j} \right\rangle & \mathbf{A}_2 \left\langle \mathrm{e}^{(-s^*-\eta) h_j} \right\rangle \\ \mathbf{B}_1 \left\langle \mathrm{e}^{(s^*+\eta) h_j} \right\rangle & \mathbf{B}_2 \left\langle \mathrm{e}^{-s^* h_j} \right\rangle \end{bmatrix}_j \begin{bmatrix} \mathbf{A}_1 & \mathbf{A}_2 \\ \mathbf{B}_1 & \mathbf{B}_2 \end{bmatrix}_j^{-1} \begin{pmatrix} \mathbf{u} \\ \mathbf{t} \end{pmatrix}_{z_j}. \tag{24}$$

Under the assumption that the displacement vector $\mathbf{u}$ and traction vector $\mathbf{t}$ are continuous across the interface, Eq. (24) can be used repeatedly. Due to the above reasons, the physical quantities can propagate from the bottom surface $z = 0$ to the top surface $z = H$ of a multilayered FGM plate. Therefore, we obtain

$$\begin{pmatrix} \mathbf{u} \\ \mathbf{t} \end{pmatrix}_H = \mathbf{E}_N (h_N) \mathbf{E}_{N-1} (h_{N-1}) \cdots \mathbf{E}_2 (h_2) \mathbf{E}_1 (h_1) \begin{pmatrix} \mathbf{u} \\ \mathbf{t} \end{pmatrix}_0, \tag{25}$$

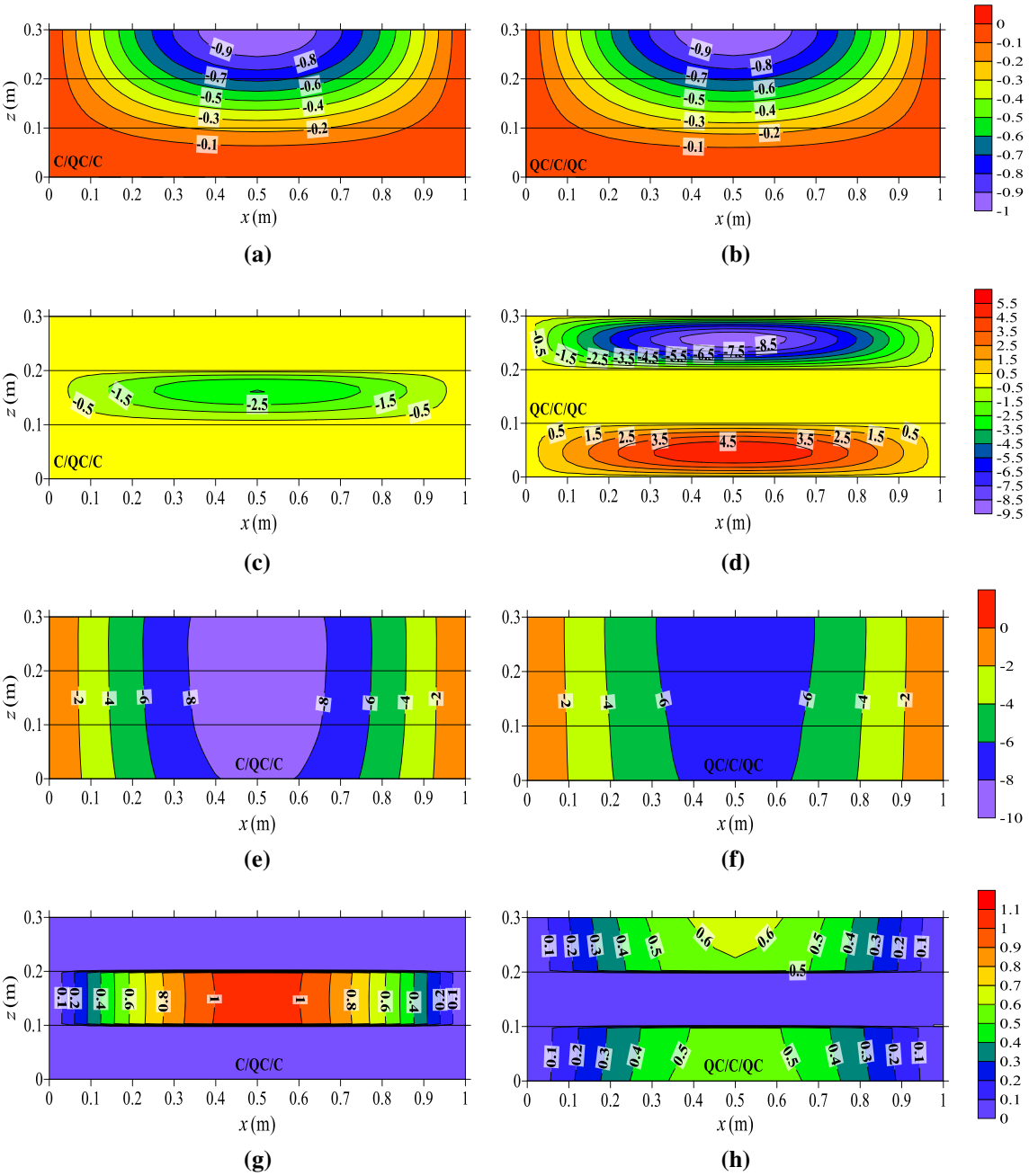

Fig. 4 Contour plots on the vertical plane ($y = 0.5L_y$) along x-direction and through z-direction with $\eta = 5$ for Sect. 4.1. **a** σ_{zz} for the C/QC/C plate (N/m^2), **b** σ_{zz} for the QC/C/QC plate (N/m^2), **c** H_{zz} for the C/QC/C plate (10^{-3} N/m^2), **d** H_{zz} for the QC/C/QC plate (10^{-3} N/m^2), **e** u_z for the C/QC/C plate (10^{-12} m), **f** u_z for the QC/C/QC plate (10^{-12} m), **g** w_z for the C/QC/C plate (10^{-12} m), **h** w_z for the QC/C/QC plate (10^{-12} m)

where

$$\mathbf{E}_k\left(h_k\right) = \begin{bmatrix} \mathbf{A}_1\left\langle \mathrm{e}^{s^* h_k}\right\rangle & \mathbf{A}_2\left\langle \mathrm{e}^{(-s^*-\eta)h_k}\right\rangle \\ \mathbf{B}_1\left\langle \mathrm{e}^{(s^*+\eta)h_k}\right\rangle & \mathbf{B}_2\left\langle \mathrm{e}^{-s^* h_k}\right\rangle \end{bmatrix}_k \begin{bmatrix} \mathbf{A}_1 & \mathbf{A}_2 \\ \mathbf{B}_1 & \mathbf{B}_2 \end{bmatrix}_k^{-1} \quad (k = 1, \ldots, N) \tag{26}$$

is called the propagator matrix. The matrices $\mathbf{A}_l$ and $\mathbf{B}_l$ ($l = 1, 2$) in the propagator matrix are normalized according to

$$-\mathbf{B}_2^{\mathrm{T}}\mathbf{A}_1 + \mathbf{A}_2^{\mathrm{T}}\mathbf{B}_1 = \mathbf{I}. \tag{27}$$

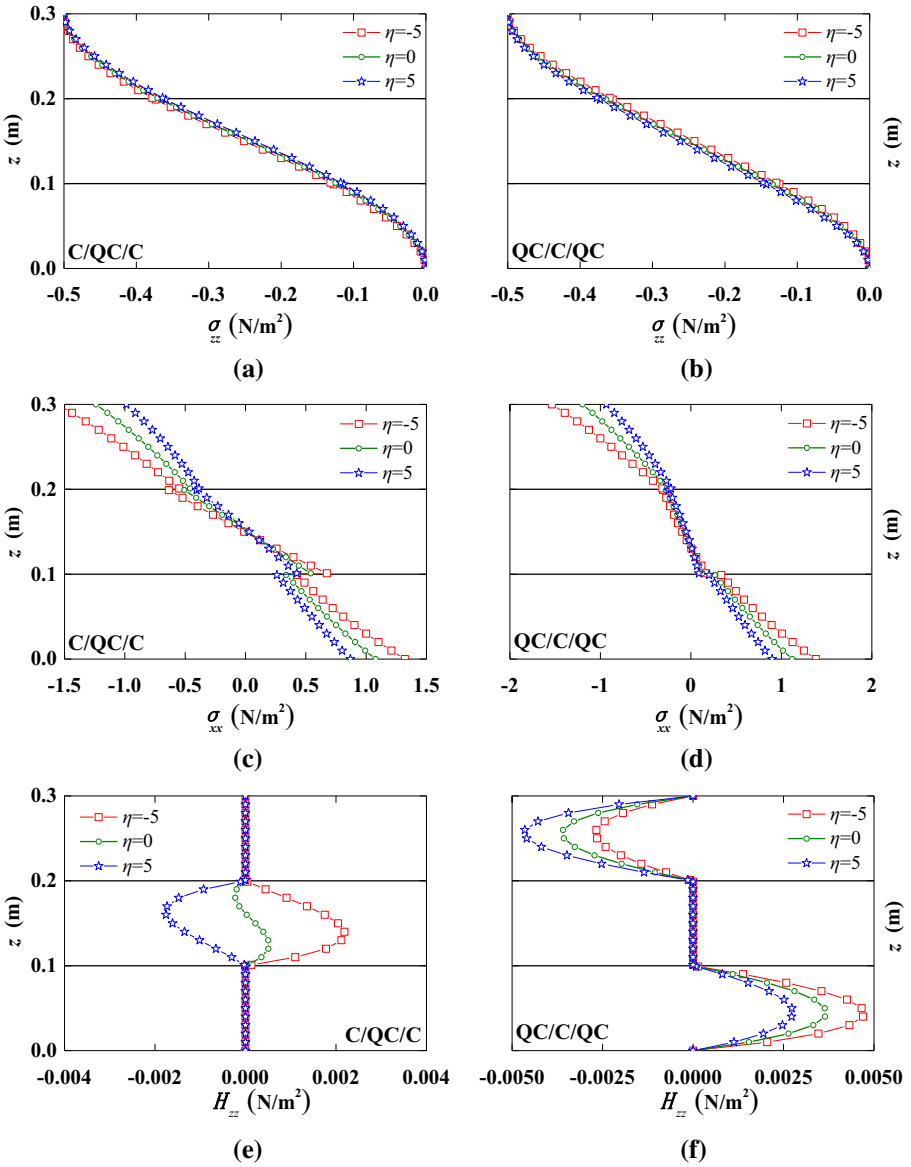

Fig. 5 Variation of the stress components with z at a location ($x = 0.75L_x$, $y = 0.75L_y$) of different η for Sect. 4.1. **a** σ_{zz} for the C/QC/C plate, **b** σ_{zz} for the QC/C/QC plate, **c** $\sigma_{xx}(=\sigma_{yy})$ for the C/QC/C plate, **d** $\sigma_{xx}(=\sigma_{yy})$ for the QC/C/QC plate, **e** H_{zz} for the C/QC/C plate, **f** H_{zz} for the QC/C/QC plate

4 Numerical examples

In this section, a multilayered FGM plate subjected to a normal force and a shear force at the top surface with simply supported boundary conditions is studied. Two different stacking sequences of the laminated plate, shown in Fig. 2, are considered. One of the stacking sequences is $BaTiO_3$/Al–Ni–Co/$BaTiO_3$ (called C/QC/C), the other sequence is QC/C/QC, which is made of Al–Ni–Co/$BaTiO_3$/Al–Ni–Co. The dimensions of a multilayered FGM plate are $L_x \times L_y \times H = 1\,\text{m} \times 1\,\text{m} \times 0.3\,\text{m}$. The three layers have equal thickness of 0.1 m. According to the material coefficients of QCs shown by Fan [23] and Sladek et al. [28], the material properties for Al–Ni–Co are listed in Table 1, and the material coefficients for $BaTiO_3$ obtained by Lee and Jiang [29] are shown in Table 2.

It is important to point out that R_m^0 and K_i^0 in the crystal are zero, on account of no phason field in classical crystalline materials [30,31]. In order to avoid generating a singular matrix, K_i^0 in the crystal is supposed to

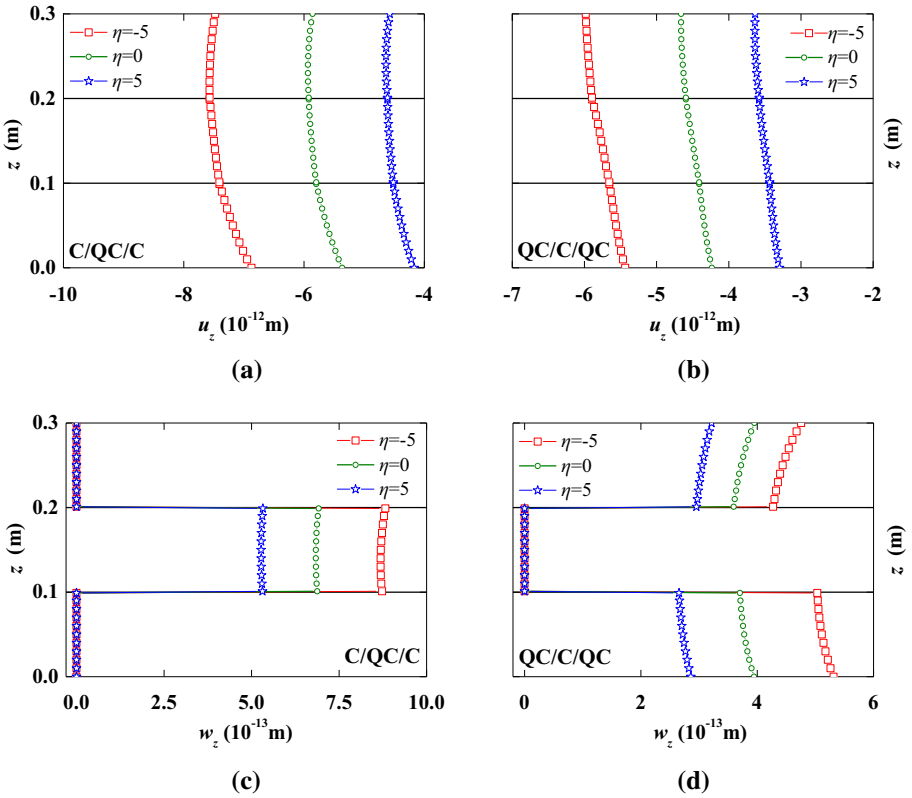

Fig. 6 Variation of the displacement components with z at a location ($x = 0.75L_x$, $y = 0.75L_y$) of different η for Sect. 4.1. **a** u_z for the C/QC/C plate, **b** u_z for the QC/C/QC plate, **c** w_z for the C/QC/C plate, **d** w_z for the QC/C/QC plate

be a very small value during the calculation, about 10^{-8} of the corresponding value of K_i^0 in QC. In addition, the phason components in Eqs. (5), (8), and (12) are zero in the crystal layer.

In the following two numerical examples, the exact solution is applied to different stacking sequences. Different load forms, which are a normal load and a shear load, respectively, are considered. The responses of physical quantities with different exponential factors are studied.

4.1 A normal load

Assuming that a multilayered FGM plate subjected to a normal load at the top surface, which takes the form

$$\sigma_{zz} = \sigma_0 \sin px \sin qy, \tag{28}$$

where σ_0 is the amplitude of the loading. Let's assume all the other traction components on the top surface and all traction components on the bottom surface are zero. Consequently, Eq. (25) can be simplified to

$$\begin{pmatrix} \mathbf{u}(H) \\ \mathbf{t}(H) \end{pmatrix} = \begin{bmatrix} \mathbf{D}_1 & \mathbf{D}_2 \\ \mathbf{D}_3 & \mathbf{D}_4 \end{bmatrix} \begin{pmatrix} \mathbf{u}(0) \\ \mathbf{0} \end{pmatrix}, \tag{29}$$

where $\mathbf{D}_1, \mathbf{D}_2, \mathbf{D}_3, \mathbf{D}_4$ are the multiplications of the propagator matrices in Eq. (25), and $\mathbf{t}(H)$ is the given traction boundary condition on the top surface, i.e.,

$$\mathbf{t}(H) = \{0, 0, \sigma_0 \sin px \sin qy, 0\}^{\mathrm{T}}. \tag{30}$$

Inserting Eq. (30) into Eq. (29), we have the unknown displacement components at the bottom surface

$$\mathbf{u}(0) = \mathbf{D}_3^{-1}\mathbf{t}(H). \tag{31}$$

Consequently, for the displacement and traction vectors at any depth, the solution is

$$\begin{pmatrix} \mathbf{u} \\ \mathbf{t} \end{pmatrix}_z = \mathbf{E}_z\left(z - z_{k-1}\right)\mathbf{E}_{k-1}\left(h_{k-1}\right)\cdots\mathbf{E}_2\left(h_2\right)\mathbf{E}_1\left(h_1\right)\begin{pmatrix} \mathbf{u} \\ \mathbf{t} \end{pmatrix}_0. \tag{32}$$

In order to investigate the response of the layered FGM plate under a normal load at the top surface with $n = m = 1$ and amplitude $\sigma_0 = -1\,\mathrm{N/m^2}$ in Eq. (28), the exponential factor η is taken as 5. It has been checked that the results in this section corresponding to the exponential factor $\eta = 0$ are exactly the same as those in Yang et al. [24].

Figure 3 presents the contour plots of the phonon stress σ_{zz} and the phonon displacement u_z at the top surface with $\eta = 5$. The contour plots of physical quantities on the $x-z$ plane at $y = 0.5L_y$ with $\eta = 5$ are shown in Fig. 4. The maximum values of σ_{zz} at the top surface, shown in Figs. 3a, b and 4a, b, are -1, and the minimum values of σ_{zz} at the bottom surface are zero. To a certain extent, according to the results of the applied traction boundary condition, the accuracy of the exact solution can be proved. It should be noted that the phonon stress σ_{zz} for the C/QC/C plate is similar to that for the QC/C/QC plate, which implies that the stacking sequence has little influence on the phonon stress σ_{zz}, because the same load along the z-direction is applied to the top surface for two different stacking sequences. The maximum values of σ_{zz} occur in the center of a multilayered plate on account of the sinusoidal loading applied, and the maximum values of the phonon displacement u_z, shown in Figs. 3c, d and 4e, f, follow the same trend. However, the maximum magnitude of u_z for the C/QC/C plate is larger than that for the QC/C/QC plate. Figures 4c, d, respectively, for the C/QC/C plate and the QC/C/QC plate, display the phason stress H_{zz}. The phason displacement w_z for both stacking sequences is shown in Figs. 4g, h. We can find that no phason stress and displacement response occur in the crystal layers. The maximum values of H_{zz} and w_z appear in the center of a multilayered plate, and the maximum values are different for two different stacking sequences. Thus, the stacking sequence plays an important role in the phason stresses and displacements, and the influence is not only on the position where the response occurs, but also on the magnitude of the physical quantities. Additionally, the physical quantities on the phonon and phason fields in Figs. 3 and 4 are symmetry with the plane of $x = 1.5\,\mathrm{m}$.

To illustrate the effect of the exponential factor on the physical components in the phonon and phason fields, a multilayered FGM plate subjected to a normal load at the top surface with three different exponential factors η, which are, respectively, $-5, 0, 5$, is studied. The horizontal coordinates are fixed at $(x, y) = (0.75L_x, 0.75L_y)$ in the analysis of the effect with different exponential factors.

Figure 5 shows the variation of the stress components in the phonon and phason fields with different η for two different stacking sequences. The values of the phonon stress σ_{zz} on the top and bottom surfaces, shown in Figs. 5a, b, satisfy the traction boundary conditions in Eq. (30), and σ_{zz} is not very sensitive to η. Figures 5c, d presents the phonon stress $\sigma_{xx}(=\sigma_{yy})$ with different η. The values of $\sigma_{xx}(=\sigma_{yy})$ increase with decreasing η. The values of H_{zz} in Figs. 5e, f are zero in crystal layers, because there is no phason field in the crystal. Moreover, the magnitude of H_{zz} for the C/QC/C plate changes by varying η from -5 to 5. The values of H_{zz} in the bottom layer for the QC/C/QC plate decrease with increasing η. Unlike the trend in the bottom layer, the change rule of phason stress H_{zz} in the top layer is contrary to that of the bottom layer. From Figs. 5a, b, e, f, it can be found that the values of stress components along the z-direction are continuous, which the agree with our hypothesis.

The phonon displacements u_z in Figs. 6a, b are continuous at the interfaces, and the magnitudes of u_z vary along with η. As for the phason displacement w_z in Figs. 6c, d, the response occurs only in the QC layers, and the values of w_z alter by varying η.

4.2 A shear load

It is assumed that a shear load is applied to a multilayered FGM plate at the top surface, i.e.,

$$\sigma_{yz} = \sigma_0 \sin px \cos qy. \tag{33}$$

The traction boundary condition at the top surface is

$$\mathbf{t}\left(H\right) = \{0, \sigma_0 \sin px \cos qy, 0, 0\}^{\mathrm{T}}. \tag{34}$$

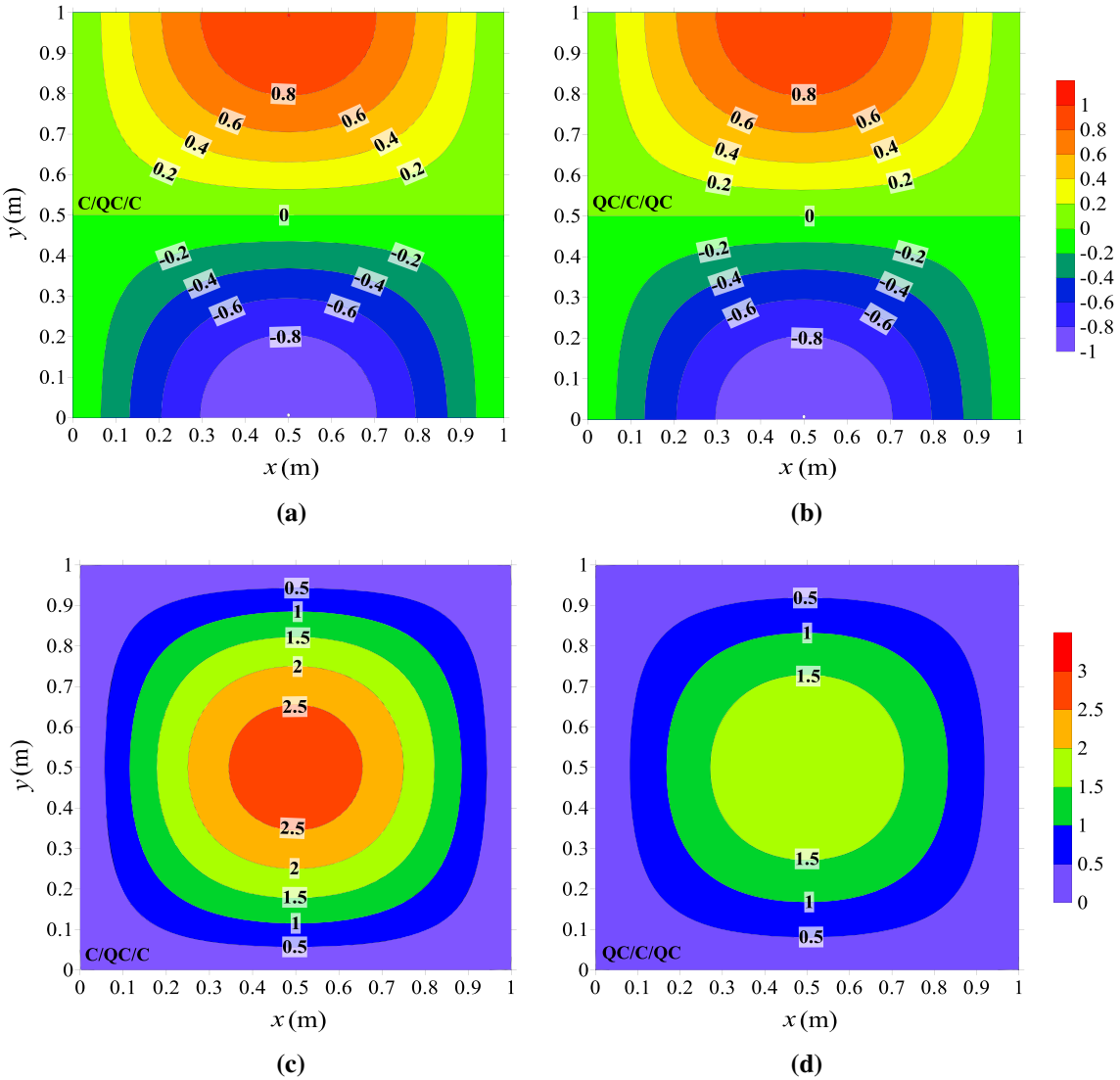

Fig. 7 Contour plots of physical quantities at the top surfaces (z = 0.3 m) subjected to a shear load with η = 5. **a** σ_{yz} for the C/QC/C plate (N/m^2), **b** σ_{yz} for the QC/C/QC plate (N/m^2), **c** u_z for the C/QC/C plate (10^{-12} m), **d** u_z for the QC/C/QC plate (10^{-12} m)

Then, substitution of Eq. (34) into Eq. (29) yields the unknown displacements at the bottom surface as

$$\mathbf{u}\,(0) = \mathbf{D}_3^{-1}\mathbf{t}\,(H)\,. \tag{35}$$

By utilizing Eq. (35) and the boundary conditions shown in Eq. (34), we can get the solution for the displacement and traction vectors, which is the same as the solution in Eq. (32).

A multilayered FGM plate subjected to a shear load with exponential factor $\eta = 5$ is analyzed in this section. The value of amplitude σ_0 is also taken for -1. The contour plots of physical quantities at the top surface, at the interfaces, and in the $y - z$ plane are presented in Figs. 7, 8 and 9, respectively.

The satisfaction of the traction boundary conditions at the top and bottom surfaces of a multilayered FGM plate can be observed from Figs. 7a, b for σ_{yz} and Figs. 9a, b, c, d, e, f for σ_{yz}, σ_{zz}, and H_{zz}. Owing to the same boundary conditions applied, no differences are found on σ_{yz} for the C/QC/C plate and QC/C/QC plate from Figs. 7a, b. It can be observed from Figs. 8a, b that the maximum values of $\sigma_{yz}$for the C/QC/C plate are greater than those for the QC/C/QC plate. The distribution of σ_{yz} in Figs. 7a, b and 8a, b is symmetry about $x = 0.5$ m and antisymmetry about $y = 0.5$ m. The responses of σ_{zz} at the interfaces and in the $y-z$ plane for

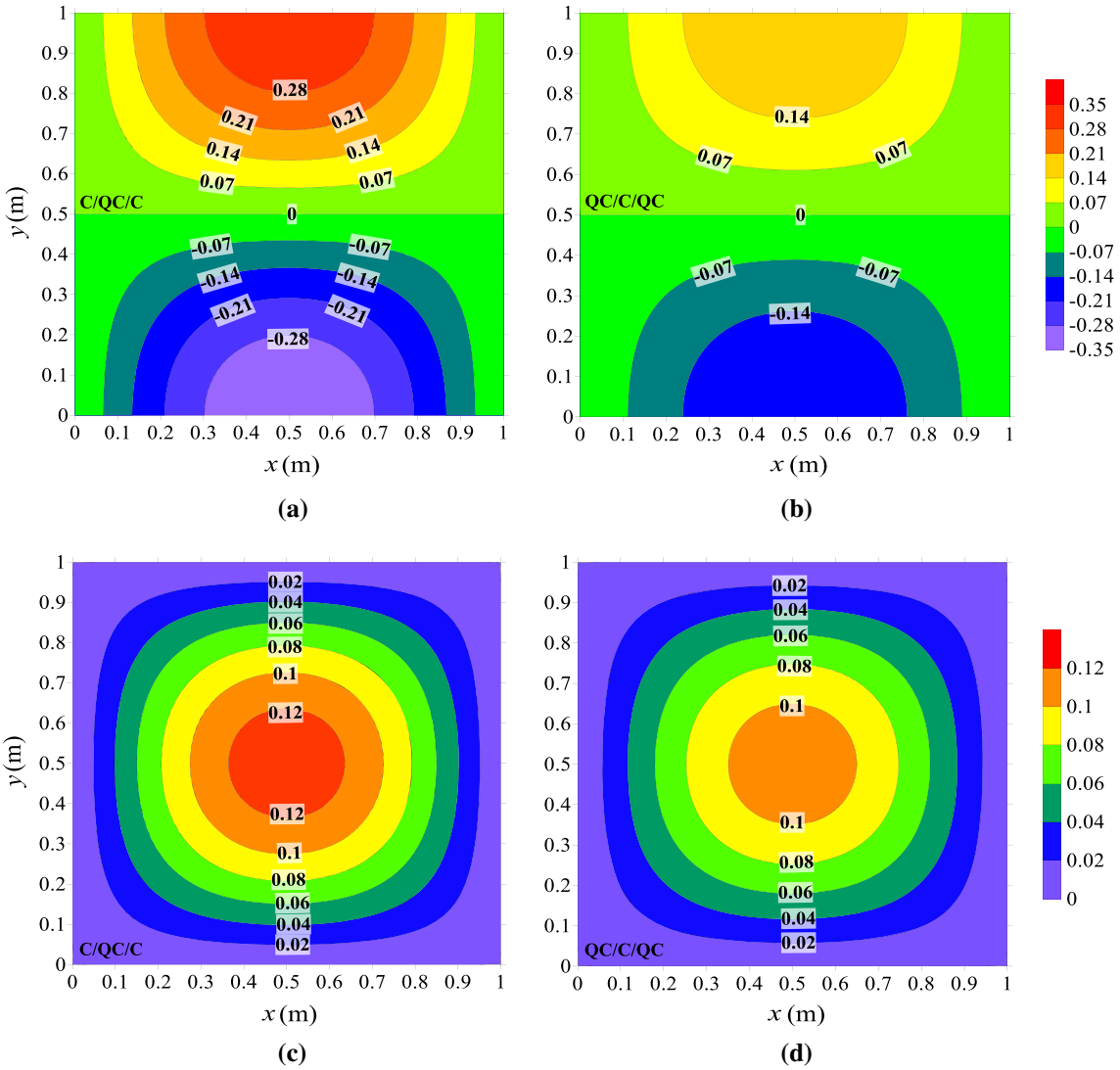

Fig. 8 Contour plots of physical quantities at the interfaces ($z = 0.2$ m) subjected to a shear load with $\eta = 5$. **a** σ_{yz} for the C/QC/C plate (N/m^2), **b** σ_{yz} for the QC/C/QC plate (N/m^2). **c** σ_{zz} for the C/QC/C plate (N/m^2), **d** σ_{zz} for the QC/C/QC plate (N/m^2)

different stacking sequences are, respectively, shown in Figs. 8c, d and 9c, d. The maximum values of σ_{zz} for the C/QC/C plate are larger than those for the QC/C/QC plate. The response on H_{zz} and w_z only exists in the QC layers, and the magnitudes of H_{zz} and w_z for the C/QC/C plate are smaller than those for the QC/C/QC plate.

Different exponential factors, i.e., $\eta = -5, 0, 5$ for the multilayered FGM plate subjected to the shear load, are also discussed in the following part. To show the physical quantities response of the plate with different η, the horizontal coordinates are fixed at $(x, y) = (0.75L_x, 0.75L_y)$.

From Figs. 10a, b, we can see that the values of σ_{yz} are zero at the bottom surface and 0.5 at the top surface. The values of σ_{zz}, shown in Figs. 10c, d, at the top and bottom surfaces are all zero, these values are consistent with the traction boundary conditions in Eq. (34). From Figs. 10e, f, there is a slight difference in the magnitude of H_{yz} with different η. The values of H_{zz} for the C/QC/C plate in Fig. 10g are zero in the crystal layers and increase with varying η from -5 to 5 in the QC layer. As for the values of H_{zz} for the QC/C/QC plate in Fig. 10h, the trend is similar to that for the C/QC/C plate. From Figs. 11a, b, the values of u_z are continuous at the interfaces. Another observation is that η has a great effect on the phonon displacement u_z. Figures 11c, d show that the phason displacement w_z is quite affected by different η.

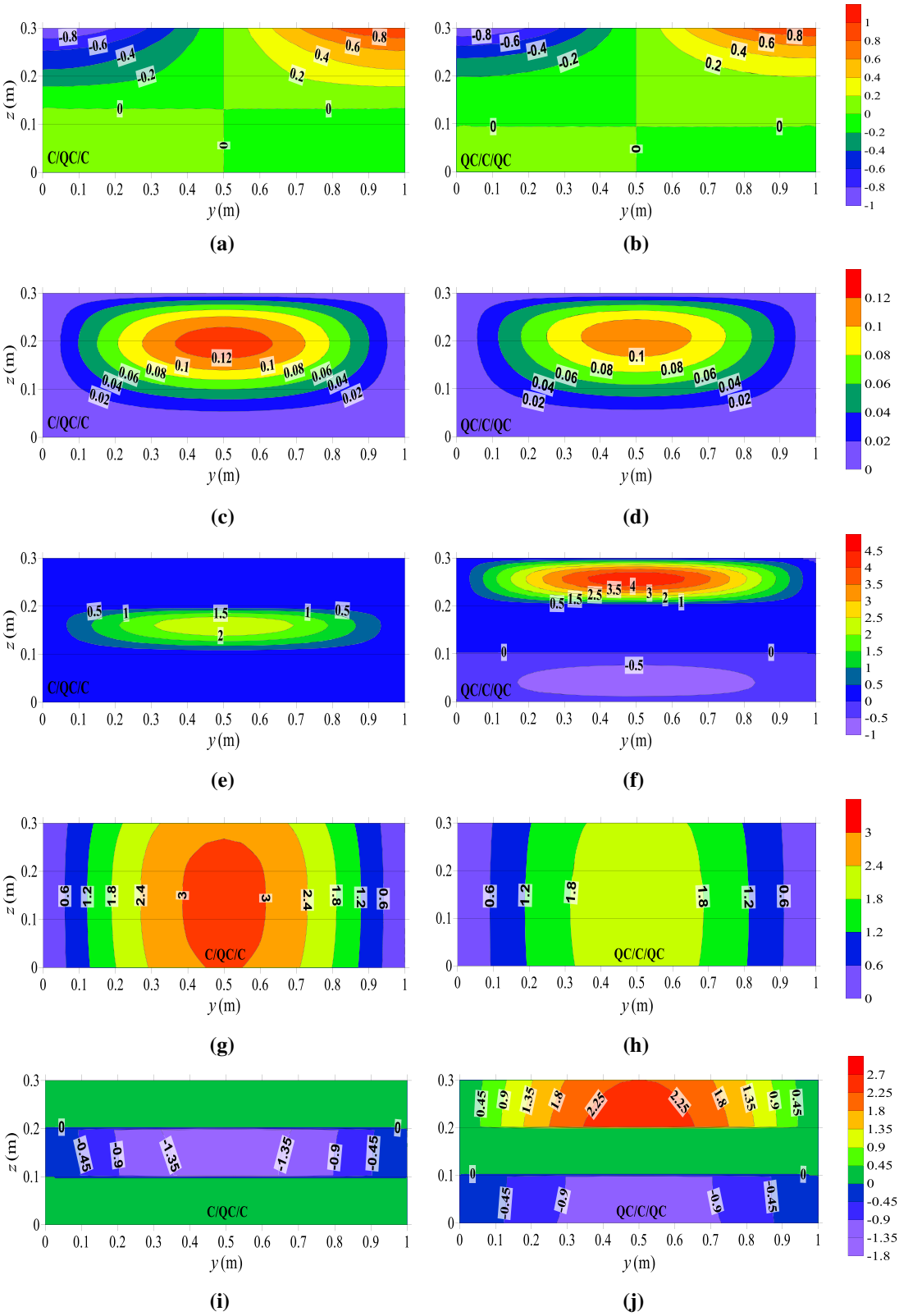

Fig. 9 Contour plots on the vertical plane ($x = 0.5L_x$) along y-direction and through z-direction with $\eta = 5$ for Sect. 4.2. **a** σ_{yz} for the C/QC/C plate (N/m^2), **b** σ_{yz} for the QC/C/QC plate (N/m^2), **c** σ_{zz} for the C/QC/C plate (N/m^2), **d** σ_{zz} for the QC/C/QC plate (N/m^2), **e** H_{zz} for the C/QC/C plate (10^{-3} N/m^2), **f** H_{zz} for the QC/C/QC plate (10^{-3} N/m^2), **g** u_z for the C/QC/C plate (10^{-12} m), **h** u_z for the QC/C/QC plate (10^{-12} m), **i** w_z for the C/QC/C plate (10^{-13} m), **j** w_z for the QC/C/QC plate (10^{-13} m)

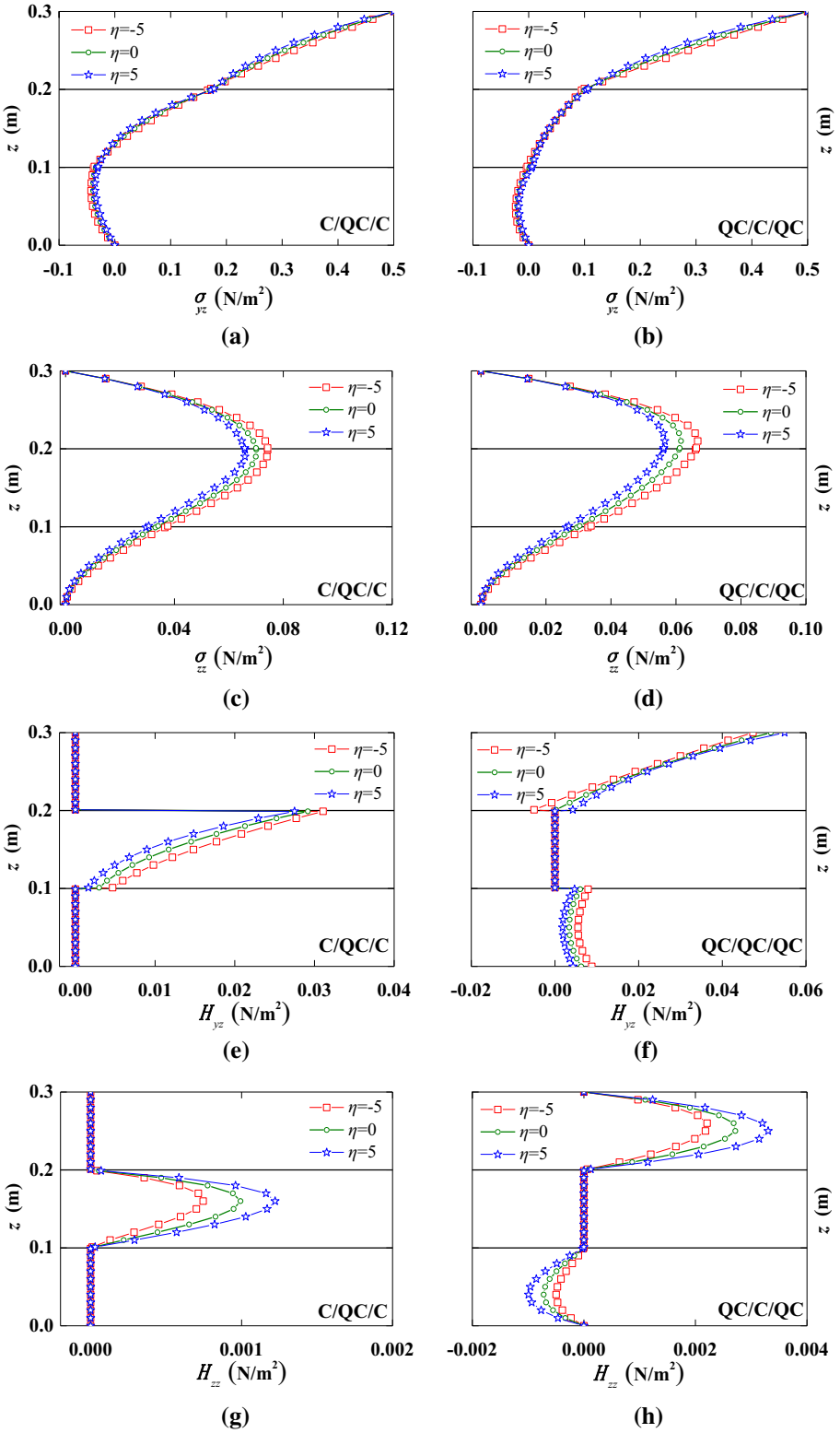

Fig. 10 Variation of the stress components with z at a location ($x = 0.75L_x$, $y = 0.75L_y$) of different η for Sect. 4.2. **a** σ_{yz} for the C/QC/C plate, **b** σ_{yz} for the QC/C/QC plate, **c** σ_{zz} for the C/QC/C plate, **d** σ_{zz} for the QC/C/QC plate, **e** H_{yz} for the C/QC/C plate, **f** H_{yz} for the QC/C/QC plate, **g** H_{zz} for the C/QC/C plate, **h** H_{zz} for the QC/C/QC plate

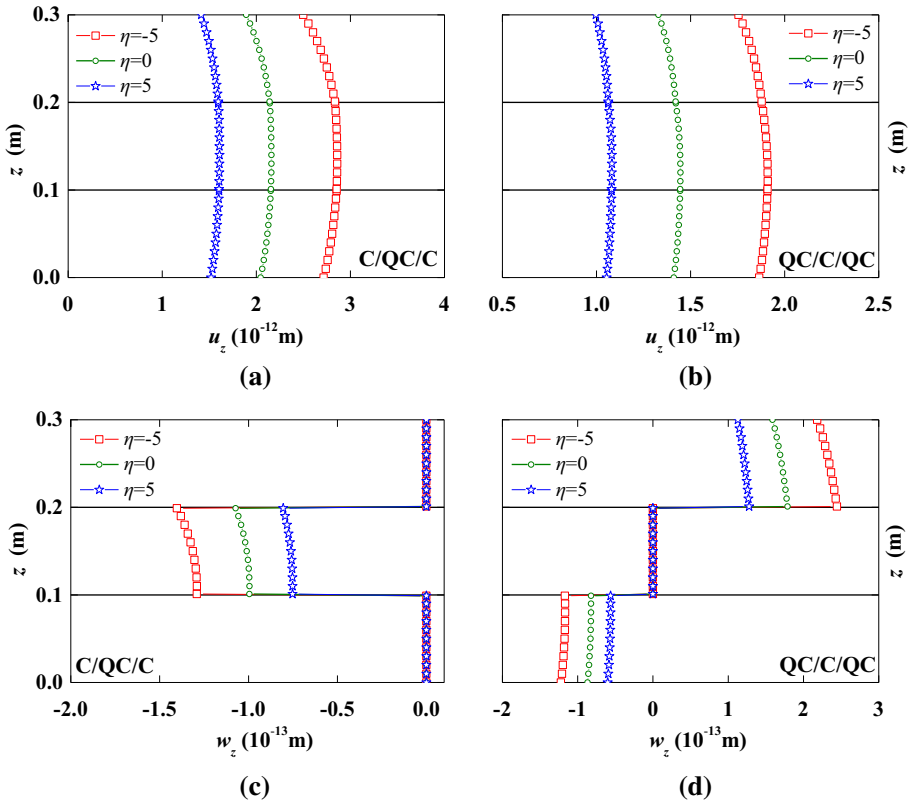

Fig. 11 Variation of the displacement components with z at a location ($x = 0.75L_x$, $y = 0.75L_y$) of different η for Sect. 4.2. **a** u_z for the C/QC/C plate, **b** u_z for the QC/C/QC plate, **c** w_z for the C/QC/C plate, **d** w_z for the QC/C/QC plate

5 Discussions and conclusions

A numerical instability may occur in the matrix calculation for layered media [32,33]. The total stresses and displacements on the system interfaces instead of reflection/transmission matrices are operated in the stiffness matrix method [32] which is unconditionally stable. Due to the adoption of a dual coordinate system, the method of reverberation-ray matrix [33] can ensure the stability of calculation for layered media. In order to verify the stability of the developed pseudo-Stroh formalism, the case of the multilayered plate subjected to a normal load with $\eta = 50$ is added in Fig. 12, which shows the variation of physical quantities of the C/QC/C plate at a fixed location ($0.75L_x$, $0.75L_y$). The satisfaction of the traction boundary conditions at the top and bottom surfaces of a layered plate can be found from Figs. 12a, b, and the value of u_z is continuous at the interfaces. It can be seen that when η is 50, the developed pseudo-Stroh formalism is numerically stable. Although numerical instability may be encountered if η is larger than 50, the case is very rare in engineering. To deal with this rare case, another modified method could be applied [34].

In this paper, an exact solution for a simply supported functionally graded multilayered 1D QC plate subjected to surface loading has been obtained by using the pseudo-Stroh formalism and propagator matrix method. In numerical results, two load forms, a normal load and a shear load, respectively, are discussed. The effects of the exponential factor η on the phonon and phason fields are compared in numerical illustrations. The influence of stacking sequence on the layered plate, and the stress condition at the interfaces for the laminated plate are also studied.

The following vital features were obtained from the numerical examples: the values of stress components and displacements in the phonon and phason fields vary with the exponential factor η; the quite different responses of physical quantities in the phonon and phason fields are induced by different load forms; all comparison studies for the stacking sequence reveal the obvious effect of it on the physical fields, especially at the interfaces of a multilayered FGM plate.

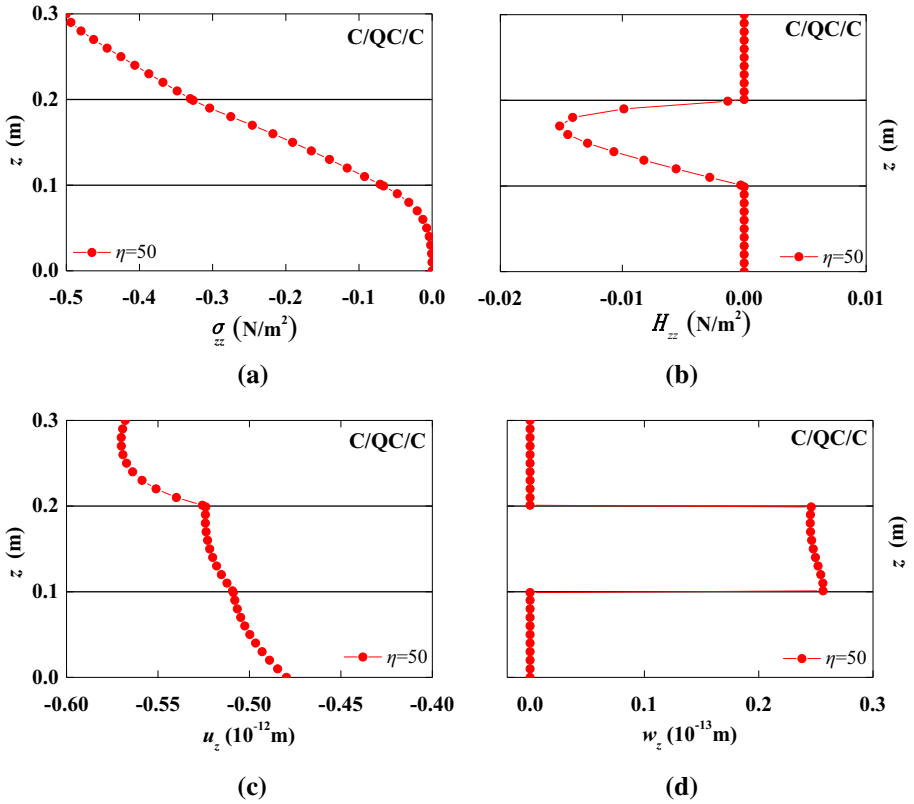

Fig. 12 Variation of the physical quantities with z at a location ($x = 0.75L_x$, $y = 0.75L_y$) of $\eta = 50$, **a** σ_{zz} for the C/QC/C plate, **b** H_{zz} for the C/QC/C plate, **c** u_z for the C/QC/C plate, **d** w_z for the C/QC/C plate

The numerical results can serve as a benchmark result for other numerical methods, and the exact solution may have potential applications in the field of smart structures based on a functionally graded multilayered 1D QC plate.

Acknowledgements The work is supported by the National Natural Science Foundation of China (Nos. 11472299 and 51704015), Program for New Century Excellent Talents in University (No. NCET-13-0552), China Agricultural University Education Foundation (No. 1101-2412001), and Dabeinong Education Foundation (No. 1101-2415002).

References

1. Shechtman, D., Blech, I., Gratias, D., Cahn, J.W.: Metallic phase with long-range orientational order and no translational symmetry. Phys. Rev. Lett. **53**, 1951–1953 (1984)
2. Ovid'ko, I.A.: Plastic deformation and decay of dislocations in quasi-crystals. Mater. Sci. Eng. A **154**, 29–33 (1992)
3. Wollgarten, M., Beyss, M., Urban, K., Liebertz, H., Köster, U.: Direct evidence for plastic deformation of quasicrystals by means of a dislocation mechanism. Phys. Rev. Lett. **71**, 549–552 (1993)
4. Levine, D., Steinhardt, P.J.: Quasicrystals: a new class of ordered structures. Phys. Rev. Lett. **53**, 2477–2480 (1984)
5. Balbyshev, V.N., King, D.J., Khramov, A.N., Kasten, L.S., Donley, M.S.: Investigation of quaternary Al-based quasicrystal thin films for corrosion protection. Thin Solid Films **447–448**, 558–563 (2004)
6. Xu, D.K., Han, E.H.: Effects of icosahedral phase formation on the microstructure and mechanical improvement of Mg alloys: a review. Prog. Nat. Sci. Mater. Int **22**, 364–385 (2012)
7. Pan, E.: Exact solution for simply supported and multilayered magneto-electro-elastic plates. J. Appl. Mech. **68**, 608–618 (2001)
8. Chen, J.Y., Chen, H.L., Pan, E.: Free vibration of functionally graded, magneto-electro-elastic, and multilayered plates. Acta Mech. Solida Sin. **19**(2), 160–166 (2006)
9. Yu, J.G., Lefebvre, J.E., Guo, Y.Q.: Wave propagation in multilayered piezoelectric spherical plates. Acta Mech. **224**, 1335–1349 (2013)
10. Guo, J.H., Chen, J.Y., Pan, E.: Analytical three-dimensional solutions of anisotropic multilayered composite plates with modified couple-stress effect. Compos. Struct. **153**, 321–331 (2016)

11. Milazzo, A.: Variable kinematics models and finite elements for nonlinear analysis of multilayered smart plates. Compos. Struct. **122**, 537–545 (2015)
12. Zhang, J., Qin, Q., Xiang, C., Wang, T.J.: Plastic analysis of multilayer sandwich beams with metal foam cores. Acta Mech. **227**, 2477–2491 (2016)
13. Fereidoon, A., Eftekhari, D., Yaghoobi, H.: Dynamic behavior of piezoelectric composite beams under moving loads. J. Compos. Mater. **50**(7), 899–916 (2015)
14. Wang, Y., Xu, R.Q., Ding, H.J.: Analytical solutions of functionally graded piezoelectric circular plates subjected to axisymmetric loads. Acta Mech. **215**, 287–305 (2010)
15. Peng, X.L., Li, X.F.: Thermoelastic analysis of functionally graded annulus with arbitrary gradient. Appl. Math. Mech. -Engl. Ed. **30**(10), 1211–1220 (2009)
16. Pan, E., Han, F.: Exact solution for functionally graded and layered magneto-electro-elastic plates. Int. J. Eng. Sci. **43**, 321–339 (2005)
17. Yan, Z., Jiang, L.Y.: Interaction of parallel dielectric cracks in functionally graded piezoelectric materials. Acta Mech. **211**, 251–269 (2010)
18. Lü, C.F., Lim, C.W., Chen, W.Q.: Semi-analytical analysis for multi-directional functionally graded plates 3-D elasticity solutions. Int. J. Numer. Methods Eng. **79**, 25–44 (2009)
19. Bian, Z.G., Chen, W.Q., Lim, C.W., Zhang, N.: Analytical solutions for single- and multi-span functionally graded plates in cylindrical bending. Int. J. Solids Struct. **42**, 6433–6456 (2005)
20. Guo, J.H., Chen, J.Y., Pan, E.: Size-dependent behavior of functionally graded anisotropic composite plates. Int. J. Eng. Sci. **106**, 110–124 (2016)
21. Zhong, Z., Wu, L.Z., Chen, W.Q.: Progress in the study on mechanics problems of functionally graded materials and structures. Adv. Mech. **40**(5), 528–541 (2010). (in Chinese)
22. Ding, D.H., Yang, W.G., Hu, C.Z., Wang, R.H.: Generalized elasticity theory of quasicrystals. Phys. Rev. B **48**, 7003–7010 (1993)
23. Fan, T.Y.: The Mathematical Elasticity of Quasicrystals and its Applications. Springer, Heidelberg (2011)
24. Yang, L.Z., Gao, Y., Pan, E., Waksmanski, N.: An exact closed-form solution for a multilayered one-dimensional orthorhombic quasicrystal plate. Acta Mech. **226**, 3611–3621 (2015)
25. Pan, E.: A general boundary element analysis of 2-D linear elastic fracture mechanics. Int. J. Fract. **88**, 41–59 (1997)
26. Pagano, N.J.: Exact solutions for rectangular bidirectional composites and sandwich plates. J. Compos. Mater. **4**, 20–34 (1970)
27. Heyliger, P.: Exact solutions for simply supported laminated piezoelectric plates. J. Appl. Mech. **64**, 299–306 (1997)
28. Sladek, J., Sladek, V., Pan, E.: Bending analyses of 1D orthorhombic quasicrystal plates. Int. J. Solids Struct. **50**, 3975–3983 (2013)
29. Lee, J.S., Jiang, L.Z.: Exact electroelastic analysis of piezoelectric laminae via state space approach. Int. J. Solids Struct. **33**, 977–990 (1996)
30. Yang, L.Z., Gao, Y., Pan, E., Waksmanski, N.: An exact closed-form solution for a multilayered two-dimensional decagonal quasicrystal plate. Int. J. Solid Struct. **51**, 1737–1749 (2014)
31. Waksmanski, N., Pan, E., Yang, L.Z., Gao, Y.: Harmonic response of multilayered one-dimensional quasicrystal plates subjected to patch loading. J. Sound Vib. **375**, 237–253 (2016)
32. Rokhlin, S.I., Wang, L.: Stable recursive algorithm for elastic wave propagation in layered anisotropic media: Stiffness matrix method. J. Acoust. Soc. Am. **112**, 822–834 (2002)
33. Pao, Y.H., Keh, D.C., Howard, S.M.: Dynamic response and wave propagation in plane trusses and frames. AIAA J. **37**(5), 594–603 (1999)
34. Pan, E.: Static Green's functions in multilayered half-spaces. Appl. Math. Model. **21**, 509–521 (1997)